Korea-Australia Rheology Journal
Vol. 21, No. 3, September 2009 pp. 193-200

Direct simulations on 2D mold-filling processes of particle-filled fluids

Wook Ryol Hwang[1,*], Worl-Yong Kim[2], Shin Hyun Kang[1] and See Jo Kim[3]
[1]*School of Mechanical and Aerospace Engineering, Research Center for Aerospace Parts Technology (ReCAPT), Gyeongsang National University, Jinju, Korea*
[2]*LG Chem/Tech Center, Daejon, Korea*
[3]*School of Mechanical Engineering, Andong National University, Andong, Korea*
(Received July 2, 2009; final version received August 14, 2009)

Abstract

We present a direct simulation technique for two-dimensional mold-filling simulations of fluids filled with a large number of circular disk-like rigid particles. It is a direct simulation in that the hydrodynamic interaction between particles and fluid is fully considered. We employ a pseudo-concentration method for the evolution of the flow front and the DLM (distributed Lagrangian multipliers)-like fictitious domain method for the implicit treatment of the hydrodynamic interaction. Both methods allow the use of a fixed regular discretization during the entire computation. The discontinuous Galerkin method has been used to solve the concentration evolution equation and the rigid-ring description has been introduced for freely suspended particles. A buffer zone, the gate region of a finite area subject to the uniform velocity profile, has been introduced to put discrete particles into the computational domain avoiding any artificial discontinuity. From example problems of 450 particles, we investigated the particle motion and effects of particles on the flow for both Newtonian and shear-thinning fluid media. We report the prolonged particle movement toward the wall in case of a shear-thinning fluid, which has been interpreted with the shear rate distribution.

Keywords : particulate flow, mold-filling simulation, buffer zone, fictitious domain method, pseudo-concentration method

1. Introduction

Solid particles are frequently added to polymeric materials to improve thermal, dielectric, mechanical properties of the solid, while retaining the processibility of the molten polymer. Particle fillers are also added to plastic as a cost-saver so that a given volume of compound requires less amount of expensive polymer (Larson, 1998). In many cases, the particulate flow is often modeled as the continuum so that the macroscopic constitutive equation could be applied to account for the particle migration and the viscosity dependence on the local particle fraction (Phillips *et al.*, 1992). The application of the model and its variant of Phillips *et al.* in the numerical simulation is quite straight forward and convenient, as its empirical parameters are universal for monodispersed spherical particle suspensions. For example, Mukhopadhyay *et al.* (2008) performed numerical simulations of concentrated particle suspensions in a wavy channel flow using the model of Phillips *et al.* (1992) to account for convected particle flux and diffusive particle flux along with the viscosity dependence on the particle fraction of the Krieger-Doherty equation (Larson 1998). Recently several modifications of the original model of Phillips *et al.* (1992) have been attempted by Kim *et al.* (2008) to consider the curvature-induced migration and they performed 2D finite element simulation to compare their new model with the experimental results. However, the necessity of individual particle-level simulations has been raised recently in developing high performance materials, based on systematic understanding of meso-scale or molecular variables in polymer processing. The presence of particles leads to micro-structural development for both particles (alignment or aggregation) and fluid (molecular conformation of polymer or crystallization) during processing due to complex particle-fluid interactions, which often alters not only the bulk suspension behavior but also the micro-rheological behavior of the fluid material. A good example is the flow-induced crystallization phenomena of the particle-filled semi-crystalline polymer during processing. The anisotropic crystallinity increases remarkably by the presence of small rigid particles and final products then can show outstanding impact toughness (Schrauwen *et al.*, 2002). Individual particle-level simulations revealed that this behavior is caused by strong extensional flows between separating particles,

*Corresponding author: wrhwang@gnu.ac.kr

which enhances the alignment of polymer molecules in the flow direction, accelerates the nucleation process, and finally results in additional impact strength in this direction (Hwang *et al.*, 2006b).

In this study, we develop numerical modeling and implementation schemes to directly simulate the 2D mold-filling process of a particulate flow formulated either with a Newtonian or a shear-thinning fluid. The term 'directly' has been used, since hydrodynamic and inter-particle interactions are fully considered in the individual particle level. To take the full hydrodynamic interaction into account, the direct numerical simulation method has several merits, since it is possible to get the velocity field affected by the particle, and moreover various constitutive models for fluid rheology can be easily combined (Hwang *et al.*, 2004a, 2004b). In addition, the treatment of free surfaces, which is essential for mold-filling simulations, in the Eulerian frame is well suited with the direct simulation technique. In this regard, we employ the direct simulation scheme of Hwang *et al.* (2004a) in the present work. The paper is organized as follows: In section 2, we introduce a simple scheme to add discrete particles continuously and present modeling schemes for direct simulations of particulate flows along with the interface evolution. Next, we present the finite-element formulation and implementation schemes including the spatial discretization and the time stepping. Then through example problems of 450 particles, we discuss particle motions and distributions during mold-filling process together with the shear-rate distribution for both Newtonian and shear-thinning fluids.

2. Modeling

As shown in Fig. 1, we consider the mold-filling process of a fluid that contains a large number of circular disk-like hard particles. We are interested in particle motions, the particle distribution and effects of freely suspended particles on the flow field. In the computational viewpoint, the problem is a difficult task, since it involves complicated hydrodynamic interactions between the fluid and particles along with the moving free surface. In this problem, we deal with the particle size of the order 1~100 μm so that both the Brownian force due to the thermal fluctuation of fluid molecules and the particle inertia could be considered

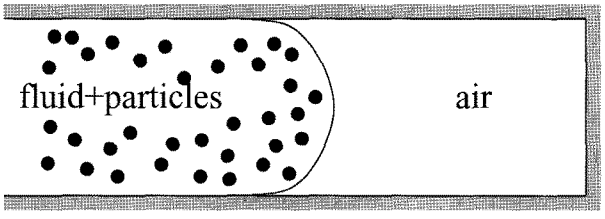

Fig. 1. A gap-wise illustration of filling of a particulate fluid inside the mold.

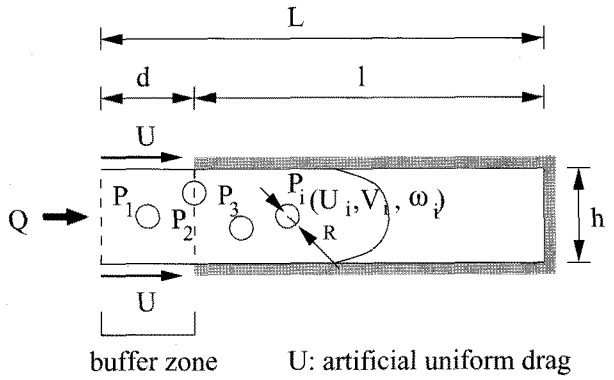

Fig. 2. A schematic depiction of the computational domain. The buffer zone is introduced in the gate region to minimize the disturbance due to the addition of discrete particles.

unimportant. In addition, for the specific application with filled polymeric liquids, which is of interest in this study, inertia for fluid, the interfacial tension between fluid and air and the contact line singularity on the wall along the interface could be also neglected (Haagh and van de Vosse, 1998).

2.1. A buffer zone

Filling simulation of a fluid with discrete particles is quite different from that of the homogeneous fluid, since discrete particles need to be added into the computational domain continuously. For this purpose, we introduce a 'buffer zone' at the inlet (the gate). The buffer zone is an artificial uniform flow region in front of the computational domain (Fig. 2). In addition to the usual inlet condition with the flow rate Q, we generate a uniform flow region by assigning the artificial uniform drag U on both upper and lower boundaries of the buffer zone. Rigid particles in the uniform flow move at the same velocity as the surrounding fluid without any rigid-body rotation and the stress shall not be generated in the buffer zone even in the vicinity of particles (except for the pressure contribution). Therefore, if a fluid is incompressible, the addition of particles into the buffer zone does not affect the remaining flow field and the discontinuity due to the discrete particle addition can be avoided. The scheme is described in Fig. 3 in detail: particles initially added to the buffer zone are transported into the remaining computational domain. When the buffer zone becomes empty, another set of particles is then introduced to the buffer zone. The time period between two addition events is denoted by t_{add} which is determined by the drag velocity U and the buffer zone length d as t_{add}>d/U, to avoid the particle overlap.

As shown in Fig. 2, the computational domain, denoted by Ω, is a straight channel with the length L and the height h, including the buffer zone of the length d. The Cartesian x and y coordinates are selected in the flow direction and in the gap-wise direction, respectively. Particles are

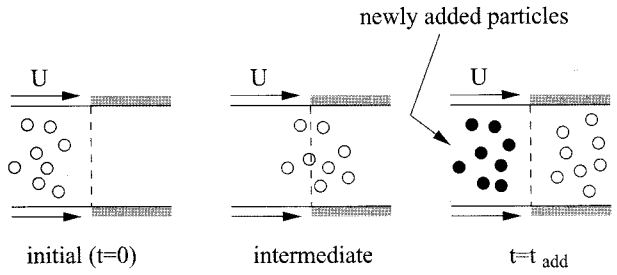

Fig. 3. The particle addition scheme inside the buffer zone. Every t_{add} time, a new set of particles are introduced into the buffer zone to avoid the particle overlap.

denoted by $P_i(t)$ (i=1,$\cdots$,N) and N is the number of particles, which increases with the particle addition. We use a symbol $P(t)$ for $\cup_{i=1}^{N} P_i(t)$, a collective region occupied by the particles at a certain time t. For a particle $P_i(t)$, $\boldsymbol{X}_i$=(X_i, Y_i), $\boldsymbol{U}_i$=(U_i, V_i), $\boldsymbol{\omega}_i = \omega_i \boldsymbol{k}$, $\boldsymbol{\Theta}_i = \Theta_i \boldsymbol{k}$ and R_i are used for the coordinates of the particle center, the translational velocity, the angular velocity, angular rotation and the radius; and $\boldsymbol{k}$ is the unit vector normal to the plane.

2.2. Solid/liquid flow

For high viscous polymeric flows, the inertia of particle and surrounding fluid is negligible and the fluid is considered incompressible. In the absence of the external body force (*e.g.* gravity), the momentum balance and the continuity equations for the domain occupied by fluid $\Omega \backslash P(t)$ are written as

$$\nabla \cdot \boldsymbol{\sigma} = \boldsymbol{0}, \quad \nabla \cdot \boldsymbol{u} = 0 \tag{1}$$

where σ is the stress tensor and $\boldsymbol{u}$ is the fluid velocity. For the constitutive equation, we employ a generalized Newtonian fluid model as

$$\boldsymbol{\sigma} = -p\boldsymbol{I} + 2\eta_f(\dot{\gamma})\boldsymbol{D}. \tag{2}$$

The quantities p, η_f, $\boldsymbol{I}$ and $\boldsymbol{D}$ are the pressure, the fluid viscosity, the identity tensor and the rate-of-deformation tensor, respectively. The shear rate $\dot{\gamma}$ is the second invariant of $2\boldsymbol{D}$, *i.e.* $(2\boldsymbol{D}:\boldsymbol{D})^{1/2}$. The Carreau-Yasuda model has been employed as a viscosity model to describe the shear-shinning behavior (Macosko, 1994):

$$\frac{\eta_f - \eta_\infty}{\eta_0 - \eta_\infty} = \frac{1}{[1+(\lambda\dot{\gamma})^a]^{(1-n)/a}}. \tag{3}$$

Following the work by Hwang *et al.* (2004a, 2004b, 2006a, 2006b), we consider the circular particle as a rigid ring, filled with the same fluid as in the fluid domain, and the rigid body condition is imposed on the particle boundary only. From the rigid-ring description, we use exactly the same set of equations for the particle domain as those of the fluid domain and it allows the implicit treatment of hydrodynamic interaction between particles and fluid. Indeed, one can use a single set of governing equations for the entire fluid domain and the discretization of the particle needs to be done only along its boundary. This fictitious domain approach is particularly useful in this work, since it is well suited with the pseudo-concentration method for the interface description using a single Eulerian mesh. The rigid-body condition on the particle boundary states that the velocity of a fluid particle attached on the particle boundary is the same as that of the particle:

$$\boldsymbol{u} = \boldsymbol{U}_i + \omega_i \boldsymbol{k} \times (\boldsymbol{x} - \boldsymbol{X}_i) \quad \text{on} \quad \partial P_i(t) \tag{4}$$

With the same governing equations with the fluid domain, the solution of this problem inside the particle is simply the rigid-body motion applied on the particle boundary extended to the full particle interior,

$$\boldsymbol{u} = \boldsymbol{U}_i + \omega_i \boldsymbol{k} \times (\boldsymbol{x} - \boldsymbol{X}_i) \quad \text{in} \quad P_i(t) \tag{5}$$

In addition, the movement of particle is given by the kinematical equations

$$\frac{d\boldsymbol{X}_i}{dt} = \boldsymbol{U}_i, \quad \boldsymbol{X}_i|_{t=0} = \boldsymbol{X}_{i,0} \tag{6}$$

$$\frac{d\Theta_i}{dt} = \omega_i, \quad \Theta_i|_{t=0} = \Theta_{i,0} \tag{7}$$

Eq. (7) is completely decoupled from the other equations, since the particle is circular.

To determine the unknown particle rigid-body motion ($\boldsymbol{U}_i$, ω_i), one needs balance conditions for the drag force and the torque on the particle boundary. In the absence of inertia and external forces or torques, particles are force-free and torque-free:

$$\boldsymbol{F}_i = \int_{\partial P_i(t)} \boldsymbol{\sigma} \cdot \boldsymbol{n} ds = \boldsymbol{0}, \tag{8}$$

$$\boldsymbol{T}_i = \int_{\partial P_i(t)} ((\boldsymbol{x} - \boldsymbol{X}_i) \times \boldsymbol{\sigma} \cdot \boldsymbol{n} ds) = \boldsymbol{0}, \tag{9}$$

where $\boldsymbol{T}_i = T_i \boldsymbol{k}$ and $\boldsymbol{n}$ is a unit normal vector on the particle boundary pointing out of the particle. We did not use an artificial particle-particle collision scheme like used in Glowinski *et al.* (1999), because the particle overlap and particle/wall collision could be avoided by taking a relatively small time step and a sufficiently refined particle boundary discretization (Hwang *et al.*, 2004b).

2.3. Interface description by the pseudo-concentration method

According to Haagh and van de Vosse (1998), the interfacial tension between the polymer and air can be neglected, since the Capillary number is the order of 10^3 in the high shear injection molding process due to its high viscosity, and the interfacial condition can be easily incorporated with the momentum equation, if described in the context of the pseudo-concentration method. As mentioned, the pseudo-concentration method is well suited with our particle description method, since both the methods are based on the Eulerian description with a fixed reg-

ular mesh over the entire computation.

In the pseudo-concentration method, the fluid and air can be identified by the concentration function $\phi \in \Omega$ that indicates the fraction of fluid material: *i.e.*, $\phi = 1$ for the fluid, while $\phi = 0$ for the air domain. The interface is identified by the level set of $\phi = 0.5$. The concentration of the material should be advected passively under given flow fields and therefore the evolution of the concentration function in the Eulerian frame is expressed as:

$$\frac{\partial \phi}{\partial t} + \boldsymbol{u} \cdot \nabla \phi = 0 \tag{10}$$

The viscosity over the entire domain is now denoted by η^*:

$$\eta^* = \phi \eta_f + (1-\phi)\eta_{air} \tag{11}$$

In this work, we use a constant air viscosity η_{air} with the order of 10^{-3} to minimize the fictitious effect of air domain on the fluid flow. In the context of the pseudo-concentration method, one can use the continuity and momentum balance equations as described in Eq. (1) and the constitutive relation for both fluid and air needs to be replaced by

$$\boldsymbol{\sigma} = -p\boldsymbol{I} + 2\eta^*(\dot{\gamma}, \phi)\boldsymbol{D} \tag{12}$$

As for the boundary condition, we assign the constant inlet velocity U on the inlet surface of the buffer zone and the no-slip condition has been applied on the mold wall attached to the fluid, while the traction free condition applied on the mold wall in the air domain. The inflow condition for ϕ on the inlet is given by '1' and the buffer zone is initially filled with the fluid material: *i.e.*, $\phi|_{t=0} = 1$ inside the buffer zone.

3. Numerical Methods

Following the combined weak formulation of Glowinski *et al.* (1999) in which the hydrodynamic force and torque acting on the particle boundary cancel exactly, Hwang *et al.* (2004a) derived a weak form with the rigid-ring description of the particle in the sliding bi-periodic computational domain. The modification of the weak form for the present problem with the pseudo-concentration method is trivial and therefore we present the final weak form without detailed derivation as follows:

For t, find such that $(\boldsymbol{u}, p, \lambda^{p,i}, \boldsymbol{U}_i, \omega_i)$ $(i=1,\cdots,N)$ such that

$$-\int_\Omega p(\nabla \cdot \boldsymbol{v})dA + \int_\Omega 2\eta^*(\dot{\gamma}, \phi)\boldsymbol{D}(\boldsymbol{u}) : \boldsymbol{D}(\boldsymbol{v})dA + \sum_{i=1}^{N} \int_{\partial P_i} \lambda^{p,i} \cdot [\boldsymbol{v} - \{\boldsymbol{V}_i + \xi_i \boldsymbol{k} \times (\boldsymbol{x} - \boldsymbol{X}_i)\}]ds = 0 \tag{13}$$

$$\int_\Omega q(\nabla \cdot \boldsymbol{u})dA = 0 \tag{14}$$

$$\int_{\partial P_i} \mu^{p,i} \cdot [\boldsymbol{u} - \{\boldsymbol{U}_i + \omega_i \boldsymbol{k} \times (\boldsymbol{x} - \boldsymbol{X}_i)\}]ds = 0, \ \forall i = 1, \cdots, N, \tag{15}$$

$$\int_\Omega \psi\left(\frac{\partial \phi}{\partial t} + \boldsymbol{u} \cdot \nabla \phi\right)dA - \sum_e \int_{\Gamma_e^{in}} \psi(\phi - \phi^{ext})(\boldsymbol{u} \cdot \boldsymbol{n}_e)ds = 0 \tag{16}$$

for all $(\boldsymbol{v}, q, \mu^{p,i}, \boldsymbol{V}_i, \xi_i, \psi)$ with $\phi|_{t=0} = \phi_0$. In Eq. (16), $\boldsymbol{n}_e$ is the outward unit normal vector on the boundary of element e, Γ_e^{in} is the part of element boundary where $\boldsymbol{u} \cdot \boldsymbol{n}_e < 0$ (inflow), and ϕ^{ext} is the concentration function value in the neighboring upwind element. In the combined weak form, the rigid-body constraint is enforced by the constraint equation using the Lagrangian multiplier on the particle boundary in Eqs. (13) and (15), $\lambda^{p,i} \in L^2(\partial P_i)$, and the discontinuous Galerkin method has been applied for the convection-dominant problem of the concentration evolution equation (Eq. 16). The discontinuous Galerkin method, which uses discontinuous interpolation of the concentration, is particularly suited in this simulation not only because of minimal coupling between elements, but also because of the inherent discontinuous nature of the interface in the Eulerian frame, as was discussed in Hwang *et al.* (2004b).

For the discretization of the weak form, we use regular quadrilateral elements over the entire domain with the continuous bi-quadratic interpolation (Q_2) for the velocity $\boldsymbol{u}$, the discontinuous linear interpolation (P_1) for the pressure p and the discontinuous bi-linear interpolation (Q_2^d) for the concentration function ϕ. Similarly to the concentration function, the use of the discontinuous interpolation of the pressure appears to be mandatory, since an arbitrary location of a particle boundary induces discontinuity in the pressure across the boundary (2004a, 2004b, 2006a).

The point collocation method has been used for equations for the rigid-ring constraint in Eqs. (13) and (15): *e.g.*

$$\int_{\partial P_i} \mu^{p,i} \cdot [\boldsymbol{u} - \{\boldsymbol{U}_i + \omega_i \boldsymbol{k} \times (\boldsymbol{x} - \boldsymbol{X}_i)\}]ds \sqcup \sum_{k=1}^{M_i} \mu_k^{p,i} \cdot [\boldsymbol{u}(\boldsymbol{x}_k) - \{\boldsymbol{U}_i + \omega_i \boldsymbol{k} \times (\boldsymbol{x}_k - \boldsymbol{X}_i)\}] \tag{17}$$

where M_i, $\boldsymbol{x}_k$ and μ_k are the number of collocation points on ∂P_i, the position of the k-th collocation point, and the Lagrangian multiplier at the collocation point, respectively. We define uniformly distributed collocation points on the particle boundary and the number of collocation points is chosen proportional to the particle radius. Approximately one collocation point in an element appears to give the most accurate result (2004a). A schematic finite-element mesh is presented in Fig. 4 along with the collocation points on the particle boundary. In actual simulations, the particle is twice of the element size.

At $t = 0$, the concentration function is initialized by ϕ_0 over the domain and the initial particle position $\boldsymbol{X}_i$ for $i=1, \cdots, N$. Then at every time step the following procedures are conducted.

Step 1 (Augmented Stokes problem) Given the concentration distribution ϕ^n and the particle position $\boldsymbol{X}_i^n$, we solve the momentum equation with the rigid-ring con-

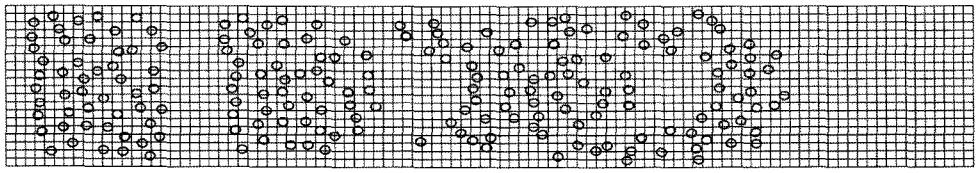

Fig. 4. A schematic finite-element mesh with the collocation points on the particle boundary.

straint (Eqs. 13~15) to get the fluid velocity (including air) and particle velocity $\boldsymbol{u}^n, p^n, \boldsymbol{U}_i^n, \omega_i^n$. An equation with a sparse symmetric matrix with many zeros on the diagonal appears at this step, which has been solved by a direct method based on the sparse multi-frontal variant of the Gaussian elimination (HSL2002/MA41).

Step 2 (Convection problem) Given the fluid velocity $\boldsymbol{u}^n$, we get the concentration function ϕ^{n+1} by integrating the evolution equation of Eq. (16). For the time stepping at this step, we employ the explicit third-order accurate TVD-RK3 (Total-Variance-Diminishing/3rd-order Runge-Kutta) scheme (Shu and Osher, 1988; Kim and Hwang, 2007):

$$\boldsymbol{M}\left(\frac{\tilde{\phi}^{n+1}-\phi^n}{\Delta t}\right)=\boldsymbol{g}(\boldsymbol{u}^n,\phi^n),$$

$$\boldsymbol{M}\left(\frac{\tilde{\phi}^{n+2}-\tilde{\phi}^{n+1}}{\Delta t}\right)=\boldsymbol{g}(\boldsymbol{u}^n,\tilde{\phi}^{n+1}),\ \tilde{\phi}^{n+0.5}=\frac{1}{4}(3\phi^n+\tilde{\phi}^{n+2}),$$

$$\boldsymbol{M}\left(\frac{\tilde{\phi}^{n+1.5}-\tilde{\phi}^{n+0.5}}{\Delta t}\right)=\boldsymbol{g}(\boldsymbol{u}^n,\tilde{\phi}^{n+0.5}),$$

$$\phi^{n+1}=\frac{1}{3}(\phi^n+2\tilde{\phi}^{n+1.5}). \tag{18}$$

The symbol $\boldsymbol{M}$ denotes the mass matrix and $\boldsymbol{g}$ is a forcing vector due to the convection term in the evolution equation of ϕ. We have also tested the 2nd order Adams-Bashforth scheme for the time stepping but TVD-RK3 has been turned out much more stable solution allowing the use of relatively large time step.

Step 3 Given the particle velocity $\boldsymbol{U}_i^n$, we update the particle position using the kinematic equation (Eq. 6) and we employ the 2nd order Adams-Bashforth method in this process. Whenever the time span between particle addition events t_{add} has passed, one needs to introduce a new set of particles into the buffer zone.

It would be worthwhile to mention the computational cost for this simulation. The example problem of a Newtonian fluid with 450 particles that will be introduced in Sec. 4 can be solved within 18 seconds per each time step with 800 MB memory using two 1.86 GHz CPU's (Intel Core Duo processor) together with a optimized BLAS (Intel Math Kernel Library).

4. Numerical Results

We add 50 circular particles every t_{add}=1 into the buffer zone of the length d=1 subject to the uniform artificial velocity U=1 until $t \le 8$. In the final time step, the total number of particles becomes 450 and the particle fraction is 9.8%. The computational domain is (L,h)=(10,1) and the particle radius R=0.025. The number of collocation points for each particle is 16 and a single particle covers four elements. Rather large number of collocation points has been applied to avoid collision between particles. We discretize the computational domain by a 400×40 finite-element mesh, employing the time step $\Delta t = 0.0025$. In Fig. 5(a), we present overall particle distribution during filling in time for a Newtonian fluid with the viscosity $\eta_f = 1$. The air viscosity η_{air} is taken as 0.001. Since each time step in Fig. 5(a) is a multiple of t_{add}, one could see the 50 particles of the same configuration in the buffer zone. As mentioned, the buffer zone is initially filled with the fluid. As time goes on, particles in the core region advance to the flow front and then move toward the wall direction, which is a typical behavior of the fountain flow. The flow front shape appears not exactly circular but is disturbed by the presence of freely suspended particles.

In order to understand the particle motion and the consequent particle distribution, we presented in Fig. 5(a) particle positions in time by color indexing: red for the firstly added particle set, green for the secondly added set, *etc.* In the period of $0<t<4$, one could observe that the initially randomly distributed red particles form a parabolic shape (t=3) and then are moved aside to the wall (t=4). Afterward the green particles come to the front and soon they are cleared away from the core region to the wall again, making a room for the next blue particle set. The process indicates the obvious effect of the fountain flow. As a result, the particles on the mold surface are arranged in chronological order: red particles and then green particles from the gate to the end. Looking at the vertical cross section (with the same x value), one could identify that particles are also stacked in the chronological order: in the core region are newer (added late) than those near the wall. However, as time goes on, the chronological stacking will disappear due to complicated hydrodynamic interaction near the wall, which might not be in reality due to the fast formation of the frozen layer there.

To investigate effects of shear-thinning on the particle motion in a non-Newtonian fluid, we plotted the colored particle distribution in Fig. 5(b). We use the Carreau-Yasuda model to represent the shear-thinning viscosity

Fig. 5. The colored particle distributions during filling: (a) Newtonian fluid; (b) non-Newtonian fluid with the Carreau-Yasuda model.

with $\eta_0 = 1$, $\eta_\infty = 0.2$, $\lambda = 1.6$, $n = 0.2$ and $a = 1.25$. One can observe that red particles are still present on the flow front even at $t=7$ in Fig. 5(b), which is not the case in Fig. 5(a) of a Newtonian fluid. It implies that the particle motion towards the wall is much prolonged in a shear-thinning fluid and this must be related with the plug-like flow formation at the flow front in such a fluid. The particle distribution on the mold surface is also distinct: red particles are distributed over the wider region than those in the Newtonian case; the boundary of each colored particle regions on the mold surface are less clear than in the Newtonian case. To clearly show the prolonged particle movement in a shear-thinning fluid, we presented the particle trajectories of the red (firstly added) particles in Fig. 6 for both the Newtonian and the non-Newtonian media. As expected, the particles initially located near the core region show the prolonged movement toward the wall for the Carreau-Yasuda fluid. In addition, the particle trajectory near the high-shear wall region appears very complicated due to the hydrodynamic interaction between particle and fluids and the particle-particle interaction.

In order to show detailed flow behaviors, we presented the shear rate distribution along with the perturbed velocity field at $t=8$ in Figs. 7 and 8 for the Newtonian and non-Newtonian fluid media, respectively. The perturbed velocity $\boldsymbol{u}'$ is defined as $(u-U, v)$ and is used to explicitly demonstrate the fountain flow on the flow front. In Fig. 7(a) and (b), we compared the homogeneous fluid flow and the particulate flow. While local high shear rates appear only near the contact point in the neat fluid case, one can observe in case of the particulate flow that the high shear rate region appears from place to place near the wall, especially at the inter-particle region, and that the overall level of shear rate increases as well. We remark that the high shear region is always formed in the $\pm 45^\circ$ and $\pm 135^\circ$ directions around the particle, like the suspended particle subject to the simple shear flow. The perturbed velocity field shows complicated disturbance due to the particle, but still

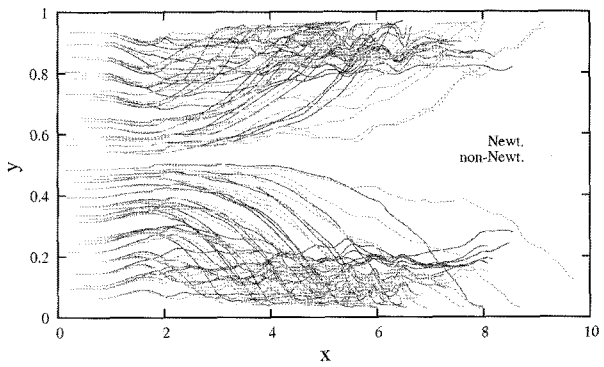

Fig. 6. Trajectories of the firstly-added 50 particles for both Newtonian (red) and shear-thinning (green) fluids.

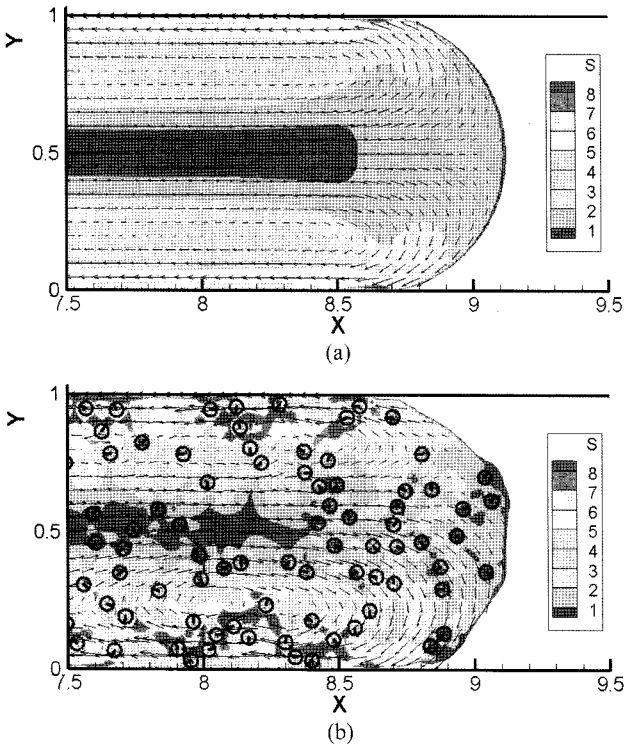

Fig. 7. The shear rate distributions and the perturbed velocity fields of (a) the non-particulate Newtonian fluid and (b) the particulate suspensions formulated with the Newtonian fluid at $t=8$.

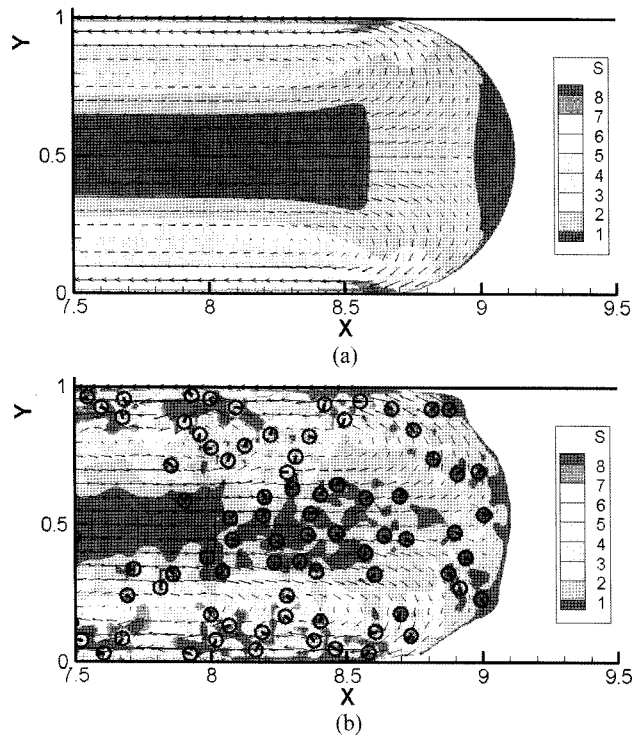

Fig. 8. The shear rate distributions and the perturbed velocity fields of (a) the non-particulate shear-thining fluid and (b) the particulate suspensions formulated with the shear-thinning fluid at $t=8$.

roughly exhibits the fountain flow pattern. In case of the non-particulate shear-thinning fluid in Fig. 8(a), large low-shear regions appear not only at the core region but also near the flow front, which indicates clearly the formation of the flat velocity profile (plug-like flow) in both regions in a shear-thinning fluid. The particle in a low shear region does not disturb the flow field much, like the extreme case already discussed in the buffer zone. Because of this fact, particles in the core region and near the flow front in Fig. 8(b) have been observed not to disturb the velocity field so much as in the case of the Newtonian medium. (The air entrapment in Fig. 8(b), the white region near the top wall, is formed during the post-processing.) Thus particles in those regions are more likely to follow the plug-like neat fluid flow pattern, from which the prolonged displacement towards the wall in a shear-thinning fluid could be interpreted. Since the shear rate near the wall is larger in the shear-thinning fluid than in the Newtonian fluid, strong particle effects near the mold wall can be expected in this case leading to higher shear rate regions in the vicinity of particles, but unfortunately we could not be able to find an evidence supporting this argument in the present simulation.

5. Conclusions

In this study, we develop numerical modeling and implementation schemes to simulate the 2D mold-filling process of a particulate flow formulated either with a Newtonian and a shear-thinning fluid using a direct simulation method in that hydrodynamic and inter-particle interactions are fully considered. Introducing the buffer zone of uniform velocity as the inlet, we could add discrete particles into the computational domain avoiding the discontinuity in the flow field. Since our particle-fluid simulation method uses a fixed Eulerian mesh, we use a pseudo-concentration method to capture the flow front between fluid and air. The highly convection-dominant concentration evolution equation has been solved using the discontinuous Galerkin and the 3rd-order accurate TVD-RK3 scheme.

From the example problem consisting of 450 particles, we investigated the particle motion and the resultant particle distribution. Particles initially located near the core region are observed to approach to the flow front and then moves toward the wall due to the (disturbed) fountain flow. As a result, particles on the mold surface are arranged in the chronological order in the case of Newtonian fluid. Using a Carreau-Yasuda fluid, we observed that the particle movement toward the wall near the flow front is prolonged in a highly shear-thinning fluid and that the chronological arrangement of particles on the mold surface is not as clear as in the Newtonian fluid case. Investigating the shear rate distribution, we found that particle effects on the flow field in the shear-thinning fluid is less dominant than in a Newtonian fluid near the flow front as well as the

core region, which is caused by the flat plug-like flow formation in the shear-thinning fluid. This weak disturbance of the particle in those regions has been turned out to be responsible for the prolonged particle movement in a shear-thinning fluid. The high shear rate induced by particles is evident in a high shear region near the wall and especially in the inter-particle region.

Of course, many important factors are dropped out in the present simulation to mimic the flow field during injection molding of particle-filled polymers. Among them, the consideration of effects of non-isothermal characteristics and the fluid viscoelasticity should be the important next step. The non-isothermal effect, especially the presence of the frozen layer, shall completely change the flow field and the particle motion. Also, viscoelasticity in the fluid is crucial to predict the particle motion correctly. For example, particle micro structural formations such as clustering and alignment are common in a viscoelastic medium and the particle motion (especially angular rotation) and the particle-fluid interaction appear quite different from those in a (generalized) Newtonian fluid, which thereby affects conformation of polymers as already demonstrated in Hwang *et al.* (2006b) in simple shear flow.

Acknowledgment

This work was supported by the Korea Research Foundation Grant funded by the Korean government (KRF-2008-008-J01001) and partially by LG Chemical Co. Ltd.

References

Glowinski, R., T.-W. Pan, T.I. Hesla and D.D. Joseph, 1999, A distributed Lagrangian multipliers/fictitious domain method for particulate flows, *Intern. J. Multiphase Flow*, **25**, 755-794.

Haagh, G.A.A.V. and F.N. van de Vosse, 1998, Simulation of three-dimensional polymer mould filling processes using a pseudo-concentration method, *Int. J. Numer. Meth. Fluids*, **28**, 1355-1369.

Hwang, W.R., M.A. Hulsen and H.E.H. Meijer, 2004a, Direct simulations of particle suspensions in a sliding bi-periodic frame, *J. Comput. Phys.*, **194**, 742-772.

Hwang, W.R., M.A. Hulsen and H.E.H. Meijer, 2004b, Direct simulations of particle suspensions of a viscoelastic fluid in a sliding bi-periodic frame, *J. Non-Newtonian Fluid Mech.*, **121**, 15-33.

Hwang, W.R. and M.A. Hulsen, 2006a, Direct numerical simulations of hard particle suspensions in planar elongational flow, *J. Non-Newtonian Fluid Mech.*, **136**, 167-178.

Hwang, W.R., G.W.M. Peters, M.A. Hulsen and H.E.H. Meijer, 2006b, Modeling of flow-induced crystallization of particle-filled polymers, *Macromolecules*, **39**, 8389-8398.

Kim, J.M., S.G. Lee and C. Kim, 2008, Numerical simulations of particle migration in suspension flows: Frame-invariant formulation of curvature-induced migration, *J. Non-Newtonian Fluid Mech.* **150**, 162-176.

Kim, S.J. and W.R. Hwang, 2007, Direct numerical simulations of droplet emulsions in sliding bi-periodic frames using the level-set method, *J. Comput. Phys.*, **225**, 615-634.

Larson, R.G., 1998, The structure and rheology of complex fluids, Oxford Univ. Press, New York.

Macosko, C.W., 1994, Rheology: Principles, Measurement and Applications, Wiley-VCH, New York.

Mukhopadhyay, S., R. Usha and E.G. Tulapurkara, 2008, Numerical study of concentrated fluid-particle suspension flow in a wavy channel, *Intern. J. Numeri. Methods in Fluids*, **59**, 1125-1155.

Phillips, R.J., R.C. Armstrong, R.A. Brown, A.L. Graham and J.R. Abbott, 1992, A constitutive equation for concentrated suspensions that accounts for shear-induced particle migration, *Phys. Fluids A*, **4**, 30-40.

Schrauwen, B.A.G., L.E. Govaert, G.W.M. Peters and H.E.H. Meijer, 2002, The influence of flow-induced crystallization on the impact toughness of high-density polyethylene, *Macromol. Symp.*, **185**, 89-102.

Shu, C.W. and S. Osher, 1988, Efficient implementation of essentially non-oscillatory shock capturing scheme, *J. Comput. Phys.*, **77**, 439-471.